Translation Initiation Factor 3 Regulates Switching between Different Modes of Ribosomal Subunit Joining

Daniel D. MacDougall and Ruben L. Gonzalez Jr.

Columbia University Department of Chemistry, *3000 Broadway, New York, NY 10027, USA*

Correspondence to Ruben L. Gonzalez: *Columbia University Department of Chemistry, 3000 Broadway, Havemeyer Hall, MC 3126, New York, NY 10027, USA. rlg2118@columbia.edu*
http://dx.doi.org/10.1016/j.jmb.2014.09.024
Edited by S. A. Woodson

Abstract

Ribosomal subunit joining is a key checkpoint in the bacterial translation initiation pathway during which initiation factors (IFs) regulate association of the 30S initiation complex (IC) with the 50S subunit to control formation of a 70S IC that can enter into the elongation stage of protein synthesis. The GTP-bound form of IF2 accelerates subunit joining, whereas IF3 antagonizes subunit joining and plays a prominent role in maintaining translation initiation fidelity. The molecular mechanisms through which IF2 and IF3 collaborate to regulate the efficiency of 70S IC formation, including how they affect the dynamics of subunit joining, remain poorly defined. Here, we use single-molecule fluorescence resonance energy transfer to monitor the interactions between IF2 and the GTPase-associated center (GAC) of the 50S subunit during real-time subunit joining reactions in the absence and presence of IF3. In the presence of IF3, IF2-mediated subunit joining becomes reversible, and subunit joining events cluster into two distinct classes corresponding to formation of shorter- and longer-lifetime 70S ICs. Inclusion of IF3 within the 30S IC was also found to alter the conformation of IF2 relative to the GAC, suggesting that IF3's regulatory effects may stem in part from allosteric modulation of IF2–GAC interactions. The results are consistent with a model in which IF3 can exert control over the efficiency of subunit joining by modulating the conformation of the 30S IC, which in turn influences the formation of stabilizing intersubunit contacts and thus the reaction's degree of reversibility.
© 2014 Elsevier Ltd. All rights reserved.

Introduction

Translation initiation is a multistep process in which a functional ribosomal complex is assembled at the start codon of a messenger RNA (mRNA) template in preparation for a new round of protein synthesis. The canonical initiation pathway in bacteria begins with binding of initiation factors (IFs) to the small, 30S, ribosomal subunit; recruitment of the mRNA and initiator formyl-methionyl transfer RNA (fMet-tRNA^{fMet}); and formation of codon–anticodon base pairing between the tRNA anticodon and mRNA start codon. The resulting intermediate, known as the 30S initiation complex (IC), can subsequently associate with the large, 50S subunit to form a 70S IC that is competent to begin peptide chain elongation [1,2]. The subunit joining step constitutes an important regulatory checkpoint during initiation, which may be up-regulated or down-regulated in order to accelerate 70S IC formation from correctly assembled 30S ICs, to prevent formation of aberrant 70S ICs containing non-initiator tRNA or incorrect start codons, and to fine-tune the efficiency of translation initiation on different mRNA templates [3–6].

The three canonical IFs, IF1, IF2, and IF3, play prominent roles in regulating the rate and fidelity of individual steps of translation initiation, including 30S IC assembly and subunit joining. Previous ensemble biochemical and biophysical studies have shown that the universally conserved GTPase IF2 facilitates recruitment and selection of fMet-tRNA^{fMet} on the 30S IC during 30S IC assembly [7,8] and subsequently accelerates subunit joining [3,4,9]. These studies have also shown that IF3 has a proofreading function during initiation, discriminating against non-canonical mRNA start codons and non-initiator tRNAs in favor of correct codon–anticodon pairing

between a canonical mRNA start codon and fMet-tRNA^{fMet} during both 30S IC assembly [7,10,11] and subunit joining [5,6]. During subunit joining, IF3 counteracts the stimulatory effect of IF2 by inhibiting the reaction to varying extents depending on the composition of the 30S IC [3–5,12]. Finally, these studies have shown that IF1 enhances the respective activities of IF2 and IF3 during 30S IC assembly and subunit joining [3,4,13,14]. The opposing effects of IF2 and IF3 on the rate of subunit joining are likely important in appropriately balancing the dual requirements of speed and accuracy during initiation [4] and may permit modulation of subunit joining efficiencies in a context-specific manner.

The stimulatory effect of IF2 on subunit joining can be attributed to the formation of favorable interactions with the intersubunit surface of the core of the 50S subunit and with components within the GTPase-associated center (GAC) of the 50S subunit [15–18], which consists of 23S ribosomal RNA helices 42–44 and ribosomal proteins L10, L11, and L7/L12. Inhibition by IF3, on the other hand, is thought to be a consequence of its binding to the "platform" domain of the 30S subunit, where it can sterically block the formation of key intersubunit interactions, termed intersubunit bridges, at the interface between the 30S and 50S subunits [19,20].

Different models have been proposed for how IF3 exerts control over subunit joining. One model posits that IF3 must dissociate from the 30S IC prior to successful subunit joining and that the rate of subunit joining is dictated by the rate of IF3 dissociation [4]. An alternate model proposes that IF1- and IF3-dependent conformational changes of the 30S IC control whether subunit joining can result in the formation of a thermodynamically stable 70S IC and that IF3 dissociation occurs subsequent to subunit joining [5]. IF3 is a structurally dynamic protein consisting of two globular domains connected by a flexible linker, which has recently been shown to adopt multiple interdomain conformations on the 30S IC that may be coupled to global conformational changes of the entire 30S IC [21]. These results lend support to the possibility that the 30S IC can undergo conformational changes that modulate the accessibility of intersubunit bridges and hence the rate of subunit joining, without requiring IF3 to dissociate. They also raise the question of whether and to what extent IF3 influences the interactions of other 30S IC components, such as fMet-tRNA^{fMet} and IF2, with the incoming 50S subunit. Addressing this question would furnish a more complete understanding of the mechanism through which IF3 regulates subunit joining.

Previous studies have demonstrated the efficacy of single-molecule fluorescence methods in characterizing conformational and temporal dynamics of the ribosome and its ligands during translation initiation [21–24]. Here, we report the use of a single-molecule fluorescence resonance energy transfer (smFRET) approach to specifically characterize the effect of IF3 on IF2-mediated subunit joining. Direct observation of individual subunit joining events has the potential to uncover structural and kinetic features underlying regulation by IF3 that have been hidden or obscured in previous ensemble-averaged measurements. Subunit joining reactions were monitored in real time based on energy transfer between fluorescence resonance energy transfer (FRET)-donor-labeled IF2 on the 30S IC and FRET-acceptor-labeled ribosomal protein L11 within the GAC. This strategy allows detection of conformational rearrangements between IF2 and the GAC during subunit joining, which have been suggested to play a functional role in this process [25,26], and permits an assessment of the extent to which the presence of IF3 on the 30S IC alters the interactions that IF2 forms with the 50S subunit.

We find that the presence of IF3 dramatically alters the dynamics of subunit joining. In the absence of IF3, subunit joining results in the formation of a highly stable, long-lifetime 70S IC. When IF3 is present within the 30S IC, however, subunit joining becomes reversible and two distinct types of subunit joining events are observed, corresponding to formation of 70S ICs with short and intermediate lifetimes and distinct distributions of relative IF2–GAC conformations. These results suggest that IF3 can exert control over subunit joining by modulating the conformation of the 30S IC and that the IF3-bound 30S IC can transition between at least two conformations that interact more weakly or more strongly with the 50S subunit. The relative occurrence of short- and intermediate-lifetime 70S ICs was found to be modulated by changes in the solution concentration of IF3 and by the use of a loss-of-function IF3 point mutant [27,28], suggesting that the equilibrium between the two 30S IC conformations can be regulated and that this could provide a mechanism to control the efficiency and fidelity of translation initiation. Thus, IF3-dependent modulation of the energetics of subunit joining may allow fine-tuning of the rate of 70S IC formation and entry into elongation within different cellular contexts and in response to different cellular cues.

Results

Development of an IF2–L11 smFRET signal to monitor subunit joining

We devised a single-molecule approach to monitor the interactions between 30S IC-bound IF2 and L11 within the GAC during real-time subunit joining reactions (Fig. 1). An IF2(S672C) point mutant was constructed and site-specifically labeled with Cy3

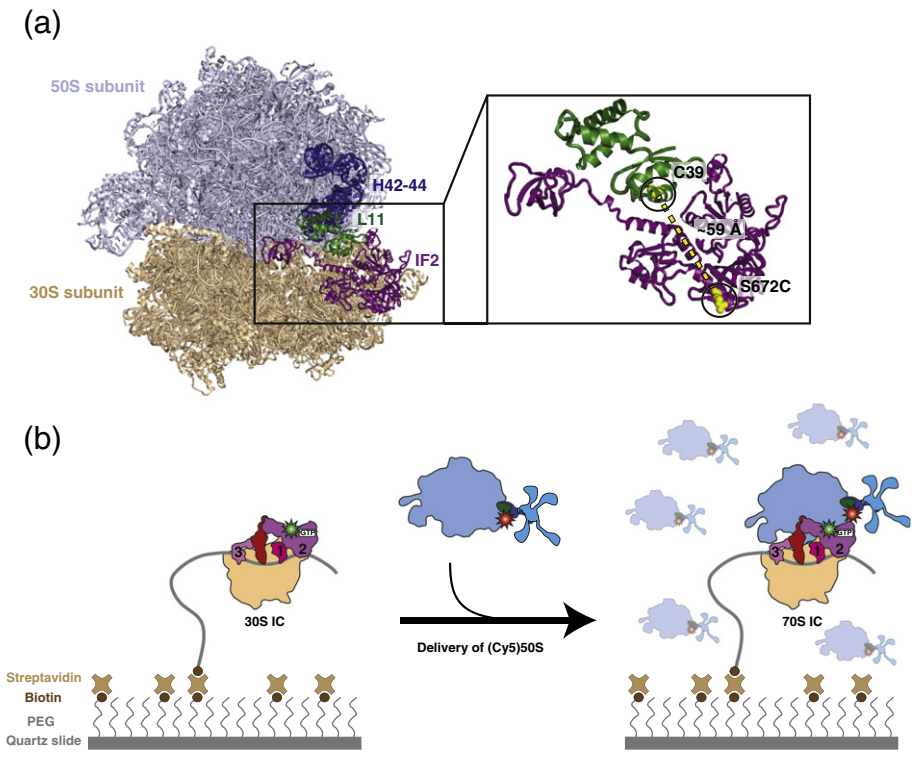

Fig. 1. Monitoring subunit joining by smFRET between L11 and IF2. (a) Left panel: Atomic model of IF2-GTP bound to the 70S IC highlighting the proximity of IF2 to the GAC. The model is based off of a cryo-EM reconstruction of a *Thermus thermophilus* 70S IC containing IF2-GMPPCP [31] (atomic coordinates kindly provided by Prof. Bruno Klaholz). Regions of the 30S and 50S subunits that were not resolved in the cryo-EM map, including L11, were added by performing structural alignments in PyMOL [34] with elements of the 30S and 50S subunits taken from an X-ray crystal structure of the *T. thermophilus* 70S ribosome (PDB IDs: 1YL3 and 1YL4). Right panel: Zoomed-in image of L11 (green) and IF2 (purple). The residues that were fluorescently labeled for smFRET measurements (C39 on L11 and S672C on IF2) are highlighted in yellow. The distance between the labeling positions was approximated by the distance between the respective α-carbon atoms. This distance was ~59 Å and is indicated by a yellow broken line. (b) Cartoon schematic of smFRET experiments. (Cy3)30S ICs were assembled on a 5′-biotinylated mRNA and tethered to the surface of a PEG-derivatized microscope slide via biotin-streptavidin interactions. Subsequently, (Cy5)50S subunits were stopped-flow delivered into the flow cell to allow formation of 70S ICs. Though not depicted in the cartoon, other initiation components were included in the buffer delivered into the flow cell (see the text for details). On the 50S subunit, L11 is shown in green and the L7/L12 stalk (not visible in the atomic model of the 70S IC) is shown in cyan.

FRET donor fluorophore to generate (Cy3)IF2. *Escherichia coli* contains three naturally occurring isoforms of IF2 (α, β, and γ) that differ in length of the N-terminus but that are each fully capable of promoting translation initiation *in vitro* [29]; a recombinant version of the γ-isoform served as the starting point for construction of (Cy3)IF2. Position S672C is located within α-helix 8 linking domains II and III of IF2 (domain numbering according to Roll-Mecak *et al.* [30]), which is expected to be in close proximity to the GAC within the 70S IC based on cryogenic electron microscopy (cryo-EM) structures [15,31] (Fig. 1a). Recombinantly expressed and purified L11 was labeled with Cy5 FRET acceptor fluorophore at its native cysteine residue (C39) within its N-terminal domain and was subsequently reconstituted into 50S subunits purified from an L11-deletion strain of *E. coli* [32,33] to generate (Cy5)50S subunits. A similar labeling scheme was used by Qin *et al.* to monitor IF2–GAC interactions with ensemble FRET techniques, except that *Bacillus stearothermophilus* IF2, labeled within the G-domain, was used in conjunction with *E. coli* 50S subunits containing L11 labeled within its N-terminal domain [26].

30S ICs bearing (Cy3)IF2 [(Cy3)30S ICs] that contained the other IFs, fMet-tRNA^{fMet}, and a 5′-biotinylated mRNA (biotin-mRNA) harboring an AUG start codon were prepared. The 5′ biotin moiety on the biotin-mRNA allows tethering of the (Cy3)30S ICs to the surface of a polyethylene glycol (PEG)-passivated and biotin-PEG-derivatized quartz microfluidic flow cell via a biotin-streptavidin-biotin bridge for visualization by total internal reflection fluorescence (TIRF) microscopy. (Cy5)50S subunits and other initiation components (variable depending on

the experiment) were stopped-flow delivered to surface-tethered (Cy3)30S ICs, and individual subunit joining events were detected based on appearance of an smFRET signal (Fig. 1b). Subunit joining triggers rapid GTP hydrolysis by IF2, which is followed by release of inorganic phosphate, transition of IF2 to its GDP-bound form, and dissociation of IF2 from the ribosome [35]. In the context of our smFRET assay, dissociation of (Cy3)IF2 from the 70S IC and its diffusion away from the TIRF-illuminated surface of the flow cell results in loss of the smFRET signal and the end of the observation window.

Subunit joining measurements were conducted in a previously described Tris-polymix buffer [21] in which we have adjusted the salt concentration such that binding of IF2 to the 70S IC is stabilized. Raising the salt concentration was found to significantly accelerate (Cy3)IF2 dissociation from the 70S IC following subunit joining (Fig. S1), indicating that electrostatic forces play an important role in stabilizing IF2–70S IC interactions. The enhanced stability of IF2 under our buffer conditions is advantageous, as it provides a longer experimental observation window that allows robust characterization of IF2–GAC conformational states accessible within the 70S IC and the identification and characterization of multiple modes of subunit joining (see below). Importantly, our initiation components are biochemically active under these buffer conditions, exhibiting levels of IF2- and ribosome-dependent GTP hydrolysis and initiation dipeptide formation that are consistent with literature values [25,35] (Figs. S2 and S3). Furthermore, fluorescent labeling of IF2 and L11 did not significantly interfere with their biochemical activity (Figs. S2 and S3).

The 50S subunit stably joins to a 30S IC lacking IF3 and the relative conformation of L11 and IF2 within the resulting 70S IC fluctuates between multiple states

IF2-mediated subunit joining was first investigated with 30S ICs containing IF1, (Cy3)IF2, GTP, fMet-tRNA^{fMet}, and biotin-mRNA but lacking IF3 [(Cy3)30S IC$_{-IF3}$]. Imaging buffer containing (Cy5)50S subunits, IF1, and GTP was stopped-flow delivered to surface-tethered (Cy3)30S IC$_{-IF3}$s, resulting in FRET efficiency (E_{FRET}) *versus* time trajectories that, upon subunit joining, exhibited a sharp transition from a state with an E_{FRET} ratio of zero (referred to as the zero-FRET state) to a state that samples one or more sub-states with distinct non-zero E_{FRET} ratios (referred to as the aggregate non-zero FRET state) (Fig. 2a). The lifetime of the zero-FRET state prior to subunit joining (τ_z) was 2.4 s at 20 nM (Cy5)50S subunits, yielding an estimated apparent bimolecular association rate constant ($k_{a,app}$) of ~21 μM^{-1} s^{-1} for subunit joining to 30S IC$_{-IF3}$ (Materials and Methods), a value that falls toward the lower end of the range of values obtained from ensemble light-scattering measurements of the rate of subunit joining to similar 30S ICs [4,12].

Subsequent to the subunit joining event, the E_{FRET} *versus* time trajectories continued to occupy the aggregate non-zero FRET state until smFRET signal loss, indicating formation of a thermodynamically stable 70S IC (Fig. 2a). Under constant laser illumination, measurement of the lifetime of the aggregate non-zero FRET state (τ_{nz}) was limited by fluorophore photobleaching. To obtain a better estimate of τ_{nz}, we extended the fluorophore survival time prior to photobleaching by shuttering the laser excitation source at regular intervals, starting after an initial 5 s of continuous data acquisition used to identify subunit joining events. As the time interval between successive frames within the shuttering regime was increased, τ_{nz} increased to values >100 s (Fig. S4 and Table S1). This corresponds to an estimate of τ_{nz} that is much less influenced by photobleaching and that likely represents the timescale of (Cy3)IF2 dissociation from the 70S IC under the current experimental conditions. This interpretation is supported by the finding that, in the presence of the non-hydrolyzable GTP analog GDPNP (guanosine-5′-[(β,γ)-imido]triphosphate), which prevents IF2 dissociation from the ribosome [36], τ_{nz}, measured using the same shuttering procedure, is increased even further to >500 s (Table S1). Taken together, these results indicate that joining of

Fig. 2. smFRET measurements of subunit joining to (a) 30S IC$_{-IF3}$ and (b) 30S IC$_{+IF3}$. First row: Cartoon illustration of experiments performed. (Cy5)50S subunits (20 nM) were stopped-flow delivered to (Cy3)30S ICs containing IF1, (Cy3)IF2, GTP, fMet-tRNA^{fMet}, biotin-mRNA, and, when included, IF3. Second row: Sample Cy3 (green) and Cy5 (red) fluorescence intensity *versus* time trajectories. Third row: The corresponding E_{FRET} *versus* time trajectories, where $E_{FRET} = I_{Cy5}/(I_{Cy3} + I_{Cy5})$. Fourth row: Time evolution of population FRET histograms, generated by superimposing hundreds of individual E_{FRET} *versus* time trajectories. The number of trajectories used to generate the histograms is indicated by "*N*". Contours are plotted from tan (lowest population, ≤1% of counts in the most populated bin) to red (highest population, ≥85% of counts in the most populated bin) according to the color bar on the left. Fifth row: TDPs were generated by plotting "Ending E_{FRET}" *versus* "Starting E_{FRET}" for all transitions between different FRET states, obtained from the idealized E_{FRET} *versus* time trajectories (see Materials and Methods), as a surface contour plot representation of a two-dimensional histogram. Contours are plotted from tan (lowest population, ≤25% of counts in the most populated bin) to red (highest population, ≥85% of counts in the most populated bin) according to the color bar on the left. The number of transitions used to generate the TDPs is indicated by "*n*".

the 50S subunit to 30S IC_{-IF3} is accompanied by formation of energetically favorable IF2–50S subunit interactions and 30S subunit–50S subunit interactions that generate a highly stable, long-lifetime ($\tau_{nz,long} \geq 100$ s) 70S IC.

Fluctuations between at least two distinct non-zero FRET states were observed within the long-lifetime 70S IC in the E_{FRET} *versus* time trajectories (Fig. 2a). A transition density plot (TDP) constructed from the smFRET data reveals that transitions most often

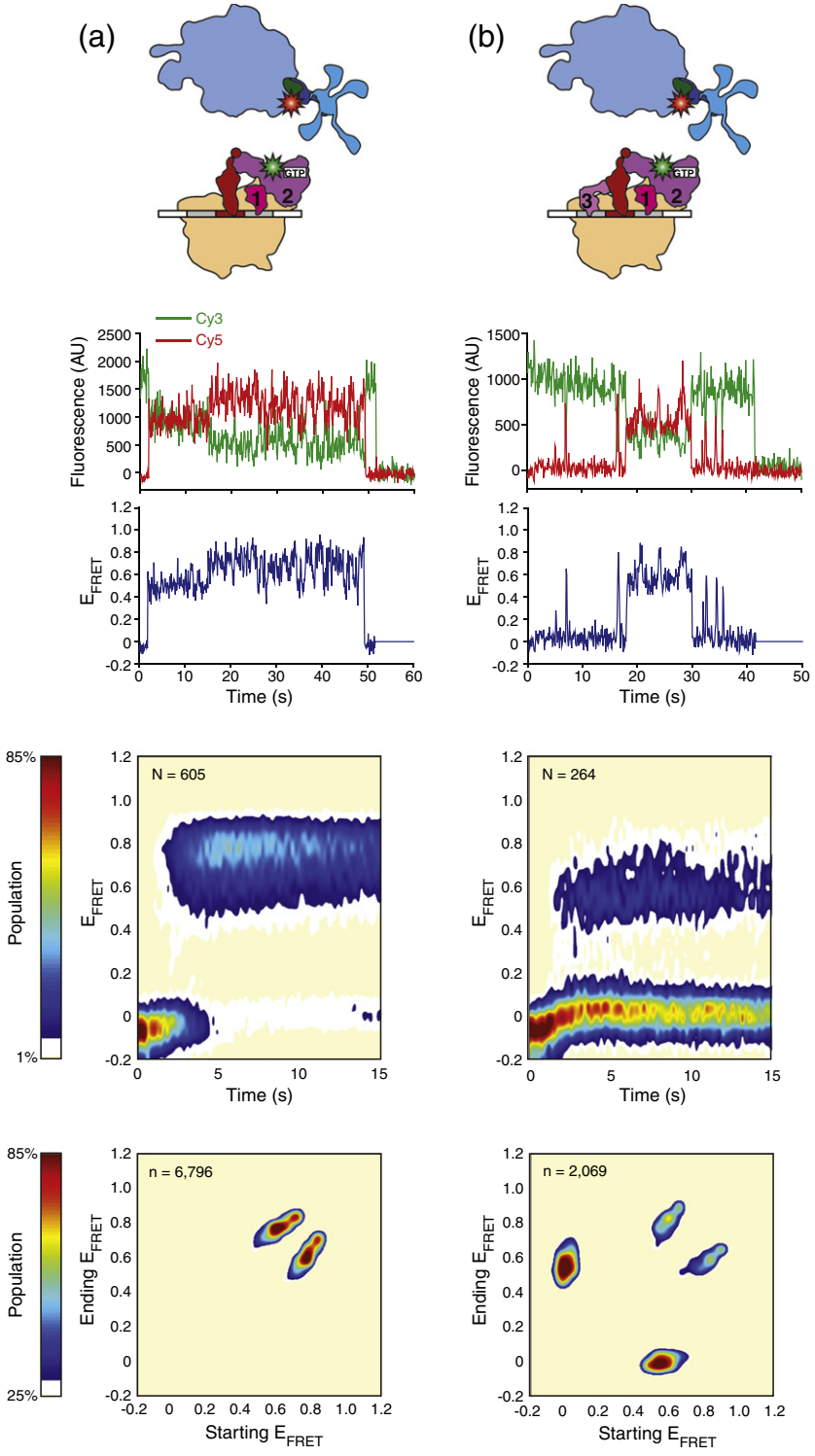

Fig. 2 (*legend on previous page*)

occur between states centered at E_{FRET} ratios of ~0.6 and ~0.8 (Fig. 2a). This indicates that there are at least two thermally accessible relative conformations of IF2 and L11 within the 70S IC and that the 70S IC can reversibly fluctuate between them. These results suggest that the intermolecular interactions between IF2 and L11 may be dynamically remodeled during subunit joining and 70S IC formation, which could entail reversible formation, reconfiguration, and/or disruption of specific intermolecular contacts. The long-lifetime 70S IC formed upon subunit joining to 30S IC_{-IF3} predominately samples the ~0.8 FRET state (Fig. 2a), which indicates that this state represents the more energetically favorable conformation of the 70S IC in the absence of IF3.

The presence of IF3 on the 30S IC alters the dynamics of subunit joining

In order to investigate how IF3 regulates interactions between the 30S IC and the 50S subunit during IF2-mediated subunit joining, we stopped-flow delivered (Cy5)50S subunits to surface-tethered (Cy3)30S ICs containing IF1, (Cy3)IF2, GTP, IF3, fMet-$tRNA^{fMet}$, and biotin-mRNA [(Cy3)30S IC_{+IF3}]. In addition to (Cy5)50S subunits, the imaging buffer that was delivered into the flow cell also contained IF1 and GTP. In the first iteration of these experiments, the imaging buffer did not contain IF3. Consequently, the majority of IF3 that was not bound to a 30S IC was flushed from the flow cell at the beginning of the experiment. The E_{FRET} *versus* time trajectories thus obtained therefore yield information on subunit joining to 30S IC_{+IF3} in the absence, or at very low concentrations, of free IF3 in the imaging buffer.

The 50S subunit reversibly joins to a 30S IC containing IF3

In contrast to the long-lifetime aggregate non-zero FRET state observed upon subunit joining to 30S IC_{-IF3}, subunit joining to 30S IC_{+IF3} resulted in the observation of shorter dwells in the aggregate non-zero FRET state and multiple transitions between the zero-FRET state and the aggregate non-zero FRET state within individual E_{FRET} *versus* time trajectories (Fig. 2b). Because transitions from the aggregate non-zero FRET state to the zero-FRET state in the E_{FRET} *versus* time trajectories predominantly result from loss of Cy5 intensity arising from the (Cy5)50S subunits rather than from the loss of Cy3 intensity from (Cy3)30S IC_{+IF3}s, these results are consistent with the reversible association of 50S subunits to 30S IC_{+IF3}, an interpretation that is in line with IF3's known anti-subunit association activity [12,37,38]. Different concentrations of (Cy5)50S subunits were stopped-flow delivered to (Cy3)30S IC_{+IF3}s in order to confirm this interpretation. As the concentration of 50S subunits was increased, τ_z decreased, as expected for a bimolecular association reaction, while τ_{nz} was independent of 50S subunit concentration, as expected for a unimolecular dissociation reaction (see Fig. 3, Fig. S5, and Table S2). Therefore, apart from instances of fluorophore photobleaching and blinking, each transition from the aggregate non-zero FRET state to the zero-FRET state represents the dissociation of a 50S subunit from 30S IC_{+IF3}, whereas each transition from the zero-FRET state to the aggregate non-zero FRET state represents binding of a 50S subunit to 30S IC_{+IF3}.

These results demonstrate that the presence of IF3 on the 30S IC can impart reversibility to the IF2-mediated subunit joining reaction. This is in agreement with a kinetic model for 70S IC formation formulated based on ensemble rapid kinetics measurements, which posits that reversible dissociation of labile 70S ICs into 30S ICs and 50S subunits can occur following initial subunit joining and GTP hydrolysis [9]. One possible explanation for the reversible subunit joining observed in our smFRET experiments is that fMet-$tRNA^{fMet}$ has dissociated from 30S IC_{+IF3} and that subunit joining cannot proceed effectively in its absence. However, control experiments performed with high concentrations of fMet-$tRNA^{fMet}$ in the imaging buffer in order to ensure the presence of fMet-$tRNA^{fMet}$ on 30S IC_{+IF3} yielded nearly identical results (Table S2), building confidence that the reversible subunit joining we observe involves complete 30S ICs containing all canonical initiation components.

The $k_{a,app}$ for subunit joining to 30S IC_{+IF3} was ~11 μM^{-1} s^{-1}, which is a modest ~1.9-fold slower than the $k_{a,app}$ for subunit joining to 30S IC_{-IF3} (~21 μM^{-1} s^{-1}). Therefore, the presence of IF3 on the 30S IC has only modest effects on the rate of initial association of the 30S IC with the 50S subunit. Instead, the primary role of IF3 appears to be to influence the stability of the 70S IC after initial association. This is consistent with a model for 70S IC formation in which IF3 exerts less of an effect on early steps and more of an effect on later steps of the subunit joining process. IF3 could affect the stability of the 70S IC directly, by sterically occluding formation of a subset of intersubunit bridges, and/or indirectly, by inducing or stabilizing 30S IC conformation(s) that make less energetically favorable interactions with the 50S subunit.

Joining of the 50S subunit to a 30S IC containing IF3 can result in the formation of two different classes of 70S IC with short and intermediate lifetimes

The individual subunit joining events observed for 30S IC_{+IF3} resulted in the formation of labile 70S ICs that exhibited highly variable dwell times in the aggregate non-zero FRET state. Inspection of individual E_{FRET} *versus* time trajectories suggested

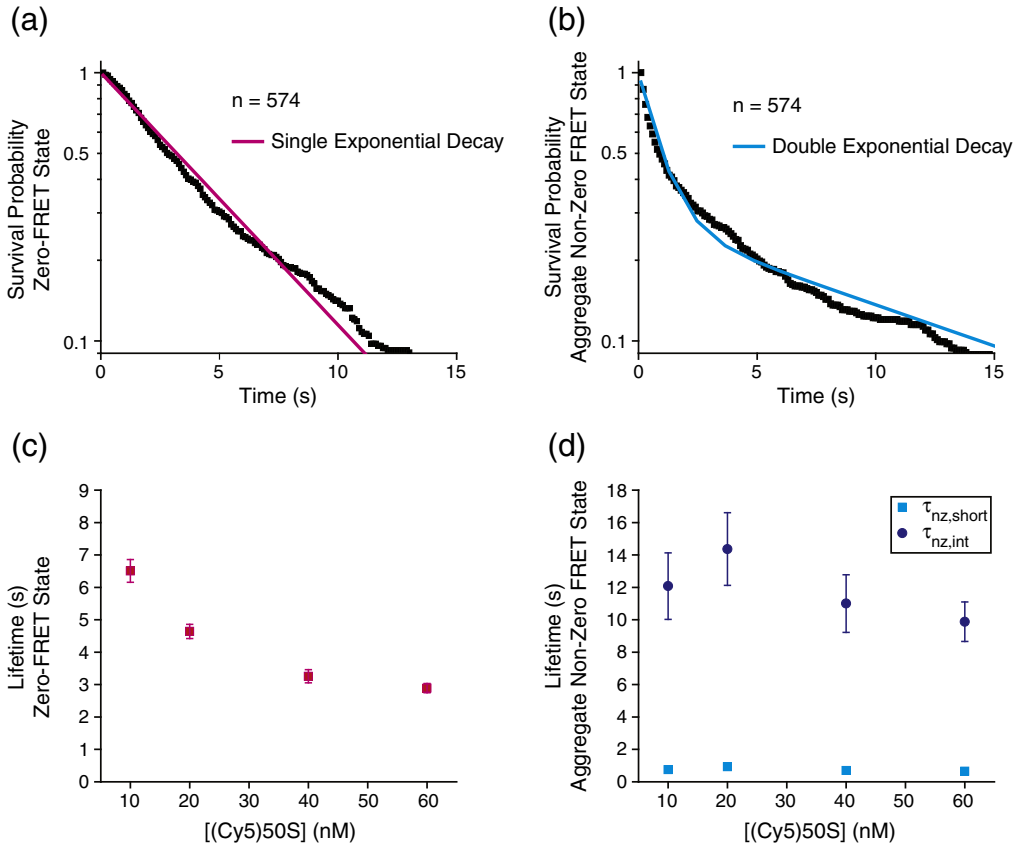

Fig. 3. Dwell-time analysis for 30S IC_{+IF3}. Top row: Survival probability plots were constructed from dwells in the zero-FRET state (a) and dwells in the aggregate non-zero FRET state (b). The sample plots shown were collected at 20 nM (Cy5)50S subunits. The number of dwells used to construct the plots is indicated by "*n*". The data were fit with exponential decays to extract the lifetimes of the respective states. The survival probability plot for dwells in the zero-FRET state was fit with a single-exponential decay (adjusted R^2 = 0.99), and the survival probability plot for dwells in the aggregate non-zero FRET state was fit with a double-exponential decay (adjusted R^2 was 0.99 when modeled with a double-exponential decay and was 0.75 when modeled with a single-exponential decay). Bottom row: Lifetimes in the zero-FRET state (c) and aggregate non-zero FRET state (d) *versus* concentration of (Cy5)50S subunits in the flow cell. Error bars were obtained by bootstrapping analysis (see Materials and Methods). The two lifetimes in the aggregate non-zero FRET state correspond to short-lifetime ($\tau_{nz,short}$) and intermediate-lifetime ($\tau_{nz,int}$) 70S ICs.

that subunit joining events may cluster into at least two distinct classes corresponding to formation of relatively short-lived and relatively long-lived 70S ICs (Fig. 2b). Accordingly, the simplest model to account for the plot of survival probabilities in the aggregate non-zero FRET state is a double-exponential decay with lifetimes of ~0.8 s and ≥10 s and amplitudes of ~0.67 and ~0.33, respectively (Fig. 3 and Table S2). The ≥10 s lifetime is likely underestimated due to fluorophore photobleaching and therefore represents a lower limit for the actual lifetime of the longer-lived 70S ICs. However, these longer-lived 70S ICs are still observed to reversibly dissociate into subunits within the experimental observation window (Fig. 2b), indicating that they are less stable compared with the long-lifetime 70S ICs formed in the absence of IF3. These results suggest that there are at least two possible modes of interaction between 30S IC_{+IF3} and the incoming 50S subunit, which result in the formation of short-lifetime ($\tau_{nz,short}$ ~ 0.8 s) or intermediate-lifetime ($\tau_{nz,int} \geq$ 10 s) 70S ICs.

To characterize the interactions between IF2 and the GAC within short- and intermediate-lifetime 70S ICs, we constructed separate histograms of E_{FRET} ratios for each (Fig. 4). For this purpose, short-lifetime 70S ICs were defined as dwells in the aggregate non-zero FRET state shorter than 4 s, and intermediate-lifetime 70S ICs were defined as dwells in the aggregate non-zero FRET state longer than or equal to 4 s. This 4-s threshold was a conservative choice that avoids contamination of the E_{FRET} distribution for intermediate-lifetime 70S ICs with E_{FRET} data from short-lifetime 70S ICs. This, in turn, allows confident assessment of not only whether the E_{FRET} distribution for intermediate-lifetime 70S ICs is different from the E_{FRET} distribution for short-lifetime 70S ICs but also whether the former is different from

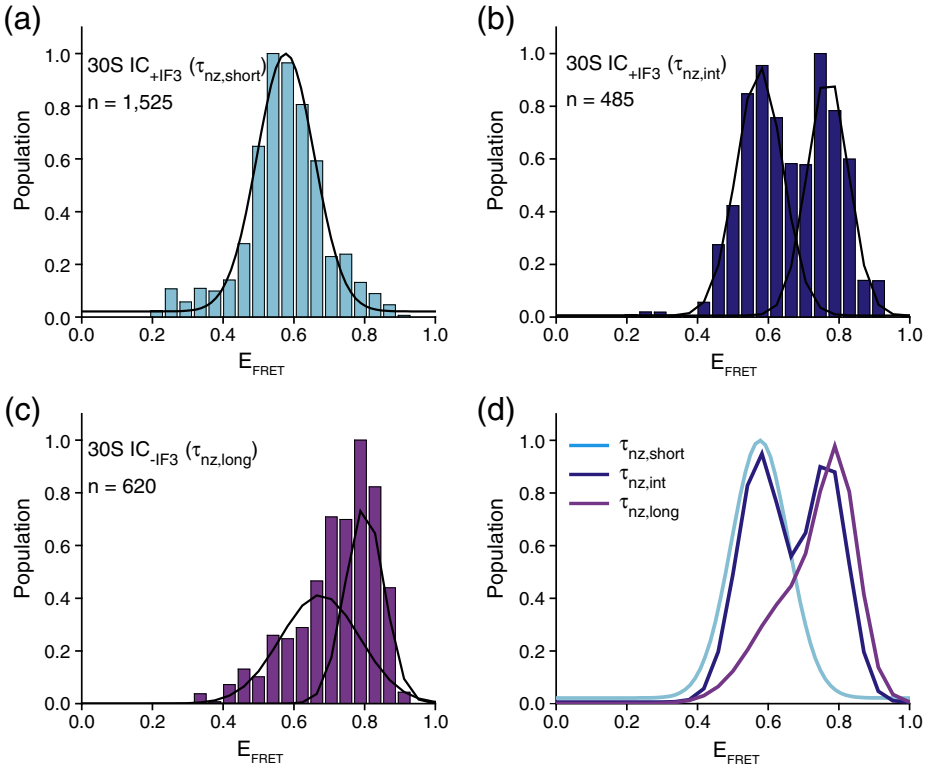

Fig. 4. Histograms of E_{FRET} ratios for 70S ICs with short, intermediate, and long lifetimes. E_{FRET} data corresponding to short-, intermediate-, and long-lifetime 70S ICs were obtained from idealized E_{FRET} *versus* time trajectories (see Materials and Methods). For 30S IC_{+IF3}, dwells in the aggregate non-zero FRET state were separated into two categories: Dwells shorter than 4 s were defined to be short-lifetime 70S ICs and dwells longer than or equal to 4 s were defined to be intermediate-lifetimes 70S ICs. The histograms of E_{FRET} ratios for short- and intermediate-lifetime 70S ICs are plotted in (a) and (b), respectively. These histograms comprise data grouped together from experiments performed at 10, 20, 40, and 60 nM (Cy5)50S subunit concentrations. For 30S IC_{-IF3}, dwells in the aggregate non-zero FRET state were defined to be long-lifetime 70S ICs and their distribution of E_{FRET} ratios is plotted in (c). The number of 70S ICs used to construct each histogram is indicated by "*n*". Black lines represent single or double Gaussian fits to the data. An overlay of the Gaussian fits is shown in (d).

the E_{FRET} distribution for the long-lifetime 70S ICs observed upon subunit joining to 30S IC_{-IF3}. Using this approach, short-lifetime 70S ICs were characterized by a single non-zero FRET state exhibiting a distribution of E_{FRET} ratios centered at ~0.6, while intermediate-lifetime 70S ICs were characterized by two non-zero FRET states exhibiting E_{FRET} ratios with peak centers at ~0.6 and ~0.8 (Fig. 4). TDPs highlight the prevalence of fluctuations between the non-zero FRET states centered at E_{FRET} ratios of ~0.6 and ~0.8 within intermediate-lifetime 70S ICs (Fig. 2b). These E_{FRET} ratios are very similar to those observed within the long-lifetime 70S ICs formed in the absence of IF3, except with different relative occupancies; in the absence of IF3, the E_{FRET} distribution is weighted toward the ~0.8 FRET state (Fig. 4). These results suggest that IF2 and L11 can adopt similar relative conformations within all 70S ICs examined but that the preferred conformation depends on the presence or absence of IF3. In other words, the presence of IF3 appears to allosterically modulate the interactions between IF2 and the GAC. Increasing 70S IC stability is correlated with a shift toward preferential population of the ~0.8 FRET state, which suggests that specific interactions between IF2 and L11 associated with the ~0.8 FRET state may play a role in influencing the stability of the 70S IC.

In summary, association of 50S subunits with 30S IC_{+IF3} can result in the formation of two classes of 70S ICs, distinguishable from each other, and 70S ICs formed in the absence of IF3, based on their unique lifetimes and distributions of relative IF2–GAC conformations. An important implication of these findings is that IF3 is likely present within both short- and intermediate-lifetime 70S ICs because dissociation of IF3 would be expected to yield 70S ICs indistinguishable from the long-lifetime 70S ICs formed upon subunit joining to 30S IC_{-IF3}. Since the intermediate-lifetime 70S ICs are stable on the ~10-s timescale, this argues against the premise that stable association of IF3 and the 50S subunit with the 30S IC are mutually exclusive.

Notably, individual 30S IC_{+IF3}s were observed to form both short- and intermediate-lifetime 70S ICs. Single 30S IC_{+IF3}s can evidently switch back and forth between these two modes of subunit joining, as formation of short-lifetime 70S ICs was observed to occur both before and after formation of intermediate-lifetime 70S ICs in individual E_{FRET} *versus* time trajectories (Fig. 2b). These data are consistent with a model in which individual 30S IC_{+IF3}s can alternate between different conformations that are more or less inhibitory toward stable association with the 50S subunit [5]. Thus, we propose that the two classes of 70S ICs observed with 30S IC_{+IF3} are reflective of an underlying conformational equilibrium of 30S IC_{+IF3}. This model assumes that individual 30S IC_{+IF3}s are compositionally homogeneous over the entire observation period, which we have attempted to ensure by including high concentrations of unlabeled initiation components in the imaging buffer. Despite this, however, the present data do not allow us to completely exclude the alternative, or additional, possibility that short- and intermediate-lifetime 70S ICs arise from changes to the composition of 30S IC_{+IF3} caused by the dissociation of unlabeled initiation components from 30S IC_{+IF3} and the rebinding of unlabeled initiation components from the imaging solution.

Free IF3 in solution suppresses formation of intermediate-lifetime 70S ICs

In the previous set of experiments, association of 50S subunits with 30S IC_{+IF3} was monitored in the absence, or at very low concentrations, of free IF3 in the imaging buffer. Therefore, the ratio of IF3 to 30S subunits was approximately one-to-one. Biochemical experiments have previously demonstrated an increase in subunit joining inhibition at high IF3-to-30S subunit molar ratios [4]. (Cy5)50S subunits were stopped-flow delivered to surface-tethered (Cy3)30S IC_{+IF3}s in imaging buffer that contained IF1, GTP, and IF3 in order to gain insight into the molecular basis for this increased inhibition (Fig. 5 and Fig. S6). The resulting E_{FRET} *versus* time trajectories revealed a preponderance of short-lived 70S ICs, with longer-lived 70S ICs being only occasionally observed (Fig. 5). As before, control experiments performed with high concentrations of fMet-$tRNA^{fMet}$ additionally included in the imaging buffer gave comparable results, strongly suggesting that the observed subunit joining events involve completely and correctly assembled 30S IC_{+IF3}s (Table S3).

Analysis of the dwell times and E_{FRET} ratios of these short-lived 70S ICs strongly suggests that they correspond to the same class of short-lifetime 70S ICs observed previously. The plot of survival probabilities in the aggregate non-zero FRET state, taking into account all subunit joining events detected with free IF3 in the imaging buffer, can be modeled with a single-exponential decay with a lifetime of ~0.8 s (Fig. 5 and Table S3). This is identical with the value of $\tau_{nz,short}$ obtained for short-lifetime 70S ICs without free IF3 in the imaging buffer and was invariant across the range of 50S subunit concentrations tested (Fig. 5 and Table S3). The goodness of fit for these single-exponential decays was only moderate for some datasets (adjusted R^2 ~ 0.9), likely reflecting the presence of a small subpopulation of longer-lived 70S ICs.

In addition to the similarity in lifetimes, the distribution of E_{FRET} ratios for all 70S ICs formed with free IF3 in the imaging buffer is highly similar to that obtained for short-lifetime 70S ICs without free IF3 in the imaging buffer. Both distributions were characterized by a single non-zero FRET state centered at an E_{FRET} ratio of ~0.6 (Fig. S7), indicative of similar modes of interaction between IF2 and the GAC. Taken together, these results indicate that subunit joining to 30S IC_{+IF3} can result in the formation of either short- or intermediate-lifetime 70S ICs and that the presence of free IF3 in solution strongly favors formation of short-lifetime 70S ICs. A titration of free IF3 over several orders of magnitude revealed that high, near-micromolar concentrations of free IF3 are required to suppress formation of intermediate-lifetime 70S ICs (Table S4).

One possible explanation for why short-lifetime 70S ICs are predominately observed in the presence of free IF3 in solution is that free IF3 binds to 50S subunits and inhibits their ability to form stabilizing interactions with 30S IC_{+IF3}. However, this explanation appears unlikely in light of the observation that the same short-lifetime 70S ICs are observed even when free IF3 is not included in the imaging buffer and is thus presumed to be present at concentrations too low to allow substantial binding to freely diffusing 50S subunits. Consequently, the data appear more consistent with a model in which 30S IC_{+IF3} can fluctuate between two conformations that favor formation of either short-lifetime or intermediate-lifetime 70S ICs and in which free IF3 in solution interacts with 30S IC_{+IF3} to bias this equilibrium toward the conformation that gives rise to short-lifetime 70S ICs. An explanation for how free IF3 could affect the dynamics of 30S IC_{+IF3}s that already contain a bound molecule of IF3 might be linked to recent studies demonstrating that free protein in solution can accelerate the turnover of a protein that is pre-bound to its binding partner [39–42] (see Discussion).

The inclusion of free IF3 in the imaging buffer did not significantly affect $k_{a,app}$ for 30S IC_{+IF3}, as similar lifetimes in the zero-FRET state were obtained in the absence and presence of free IF3 for each 50S subunit concentration tested (Tables S2 and S3). This suggests that the inhibition of 70S IC formation observed at high IF3-to-30S subunit ratios in

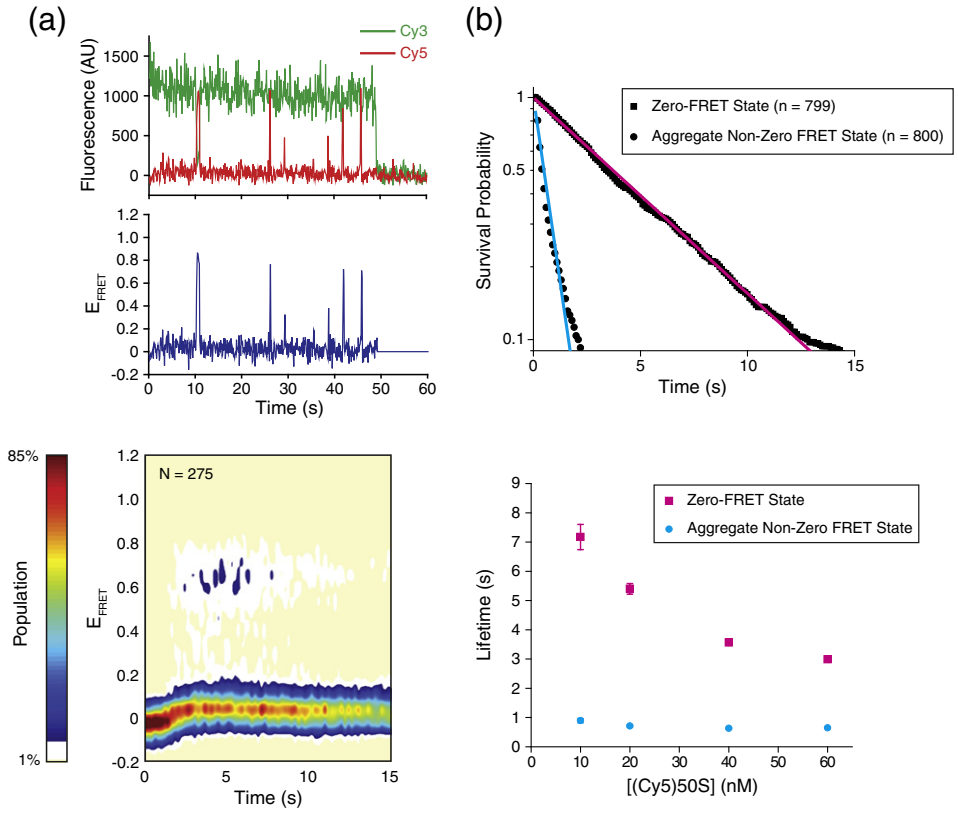

Fig. 5. Subunit joining to 30S IC_{+IF3} in the presence of free IF3. Imaging buffer containing (Cy5)50S subunits, IF1 (0.9 μM), IF3 (0.9 μM), and GTP (1 mM) was stopped-flow delivered to (Cy3)30S IC_{+IF3}. The concentration of (Cy5)50S subunits was varied from 10 to 60 nM. (a) Sample smFRET data recorded with 20 nM (Cy5)50S subunits. From top to bottom: Sample Cy3 and Cy5 fluorescence intensity *versus* time trajectory, the corresponding E_{FRET} *versus* time trajectory, and time evolution of population FRET histogram. Data are plotted as in Fig. 2. (b) Dwell-time analysis of the zero-FRET state and aggregate non-zero FRET state. Top row: Sample survival probability plots from the dataset collected with 20 nM (Cy5)50S subunits. Both curves were fit with single-exponential decays (adjusted R^2 = 0.998 for dwells in the zero-FRET state, magenta line; adjusted R^2 = 0.96 for dwells in the aggregate non-zero FRET state, cyan line). Bottom row: Lifetime of the zero-FRET state and aggregate non-zero FRET state *versus* the concentration of (Cy5)50S subunits in the flow cell.

ensemble biochemical experiments [4] may arise not from defects in subunit recruitment, but rather, it may arise from the failure of 30S IC_{+IF3} to establish stabilizing interactions with the 50S subunit upon initial subunit association. More specifically, our data suggest that, at high IF3-to-30S subunit ratios, 30S IC_{+IF3} is biased toward a conformation that is capable of associating only transiently with the 50S subunit, forming short-lifetime 70S ICs that undergo rapid dissociation and hence would be non-accumulating at the ensemble level.

A loss-of-function IF3 mutant exerts differential control over subunit joining dynamics

IF3 is known to undergo interdomain conformational rearrangements on the 30S IC, which are likely facilitated by the flexible linker connecting its globular N- and C-terminal domains and that may be coupled to conformational rearrangements of the entire 30S IC [21]. We therefore wondered whether the IF3-dependent subunit joining dynamics observed here might be influenced by the interdomain conformation of IF3 on 30S IC_{+IF3}. To investigate this possibility, we made use of an IF3 point mutant, IF3(Y75N), which was identified in a genetic screen based on its inability to discriminate against initiation at non-canonical start codons [27,28]. IF3(Y75N) binds normally to 30S subunits but is defective in start codon selection and initiator tRNA selection *in vitro* and *in vivo* [28]. The Y75N point mutation is located within the linker between IF3's N- and C-terminal domains, proximal to its N-terminal domain. Recent single-molecule studies have demonstrated that the interdomain conformation of IF3(Y75N) on the 30S IC is markedly altered relative to wild-type IF3 [21].

We prepared and surface-tethered (Cy3)30S IC_{+IF3}s containing IF3(Y75N), denoted (Cy3)30S $IC_{+IF3(Y75N)}$, and monitored subunit joining upon

stopped-flow delivery of (Cy5)50S subunits either in the absence or in the presence of free IF3(Y75N) in the imaging buffer, under experimental conditions otherwise identical with those employed for the analogous experiments with wild-type IF3. The resulting E_{FRET} *versus* time trajectories exhibit reversible formation of both shorter-lived and longer-lived 70S ICs that sample non-zero FRET states centered at E_{FRET} values similar to those observed for 70S ICs formed in the presence of wild-type IF3 (Fig. 6). The plots of survival probabilities in the aggregate non-zero FRET state were well-described by double-exponential decays with lifetimes similar to or slightly longer than those observed with wild-type IF3 (Table S5). Taken together, these results suggest that 30S $IC_{+IF3(Y75N)}$ can participate in formation of either short- or intermediate-lifetime 70S ICs that resemble those formed with wild-type IF3 but that potentially possess subtle conformational and energetic differences.

Further inspection of the smFRET data indicated that intermediate-lifetime 70S ICs are formed more frequently in the presence of IF3(Y75N) than in the presence of wild-type IF3. To quantify this effect, we classified all observed dwells in the aggregate non-zero FRET state as short-lifetime 70S ICs or intermediate-lifetime 70S ICs based on a 2-s threshold (see Materials and Methods). Based on this classification, 57% of the observed subunit joining events resulted in formation of intermediate-lifetime 70S ICs for IF3(Y75N), compared with 34% of the observed subunit joining events for wild-type IF3, when free IF3 was not included in the imaging buffer. Likewise, when free IF3 was included in the imaging buffer, 22% of the observed subunit joining events resulted in formation of intermediate-lifetime 70S ICs for IF3(Y75N), compared with 10% of the observed subunit joining events for wild-type IF3. These results suggest that IF3(Y75N) renders 30S IC_{+IF3} more permissive toward stable association with the 50S subunit. Additionally, based on the location of the Y75N point mutation within IF3's molecular structure, they suggest that IF3's linker and/or N-terminal domain may play a functionally important role in regulating subunit joining dynamics.

Discussion

Our smFRET studies have revealed the existence of multiple, discrete modes of subunit joining during translation initiation. Joining of the 50S subunit to 30S IC_{-IF3} leads to the formation of a long-lifetime 70S IC, whereas joining of the 50S subunit to 30S IC_{+IF3} can result in the formation of short- or intermediate-lifetime 70S ICs (Fig. 7). Both short- and intermediate-lifetime 70S ICs were observed to undergo dissociation into free subunits, providing direct evidence that IF2-mediated subunit joining is reversible in the presence of IF3, in agreement with proposals based on ensemble rapid kinetics measurements [5,9]. The ability of IF3 to impart reversibility to the subunit joining reaction may be an important component of its fidelity function to impede formation of 70S ICs lacking initiator tRNA or containing a non-initiator tRNA and/or a non-canonical mRNA start codon [5,6,12,27,43].

We propose that the two modes of subunit joining observed in the presence of IF3 arise from distinct conformational subpopulations of 30S IC_{+IF3} with starkly different propensities for associating stably with the 50S subunit. This would imply that IF3-dependent conformational changes of the 30S IC can modulate the number and/or strength of interactions formed between the 30S IC and the 50S subunit. As a caveat, we note that the present data do not allow us to completely exclude the alternative, or additional, possibility that dissociation and rebinding of unlabeled initiation components generates compositionally heterogeneous 30S IC_{+IF3}s with different subunit joining behaviors. However, the existence of conformational subpopulations of 30S IC_{+IF3} would be consistent with reports from cryo-EM studies that the presence of IF3 increases conformational heterogeneity of the 30S IC [20,44]. It would also be in agreement with a model put forth by Milon *et al.* based on biochemical data, which postulates that the 30S IC can adopt alternate conformations that are either productive for or inhibitory toward efficient subunit joining and 70S IC formation [5]. Thus, the putative conformations of 30S IC_{+IF3} that we propose give rise to short- and intermediate-lifetime 70S ICs will be referred to hereafter as inhibitory and productive conformations, respectively. The observation that individual 30S IC_{+IF3}s are able to participate in formation of both short- and intermediate-lifetime 70S ICs suggests that 30S IC_{+IF3}s exist in a dynamic equilibrium between these inhibitory and productive conformations (Fig. 7).

Both short- and intermediate-lifetime 70S ICs presumably contain bound IF3, based on their characteristic lifetimes and E_{FRET} distributions that distinguish them from the long-lifetime 70S ICs formed in the absence of IF3. We speculate that dissociation of IF3, like dissociation of IF2, may be slowed under the currently employed buffer conditions. IF3 dissociation would be expected to enable the formation of additional intersubunit contacts and conversion of the 70S IC into a highly stable form such as that observed here upon subunit joining to 30S IC_{-IF3}. Thus, in buffers containing higher salt concentrations, we expect that the 70S ICs initially formed upon subunit joining to 30S IC_{+IF3} would result in IF3 dissociation and conversion into a morestable form at a faster rate and thus a larger fraction of the time. Exploration of this possibility is not feasible with the currently employed (Cy3)IF2–(Cy5)L11 smFRET

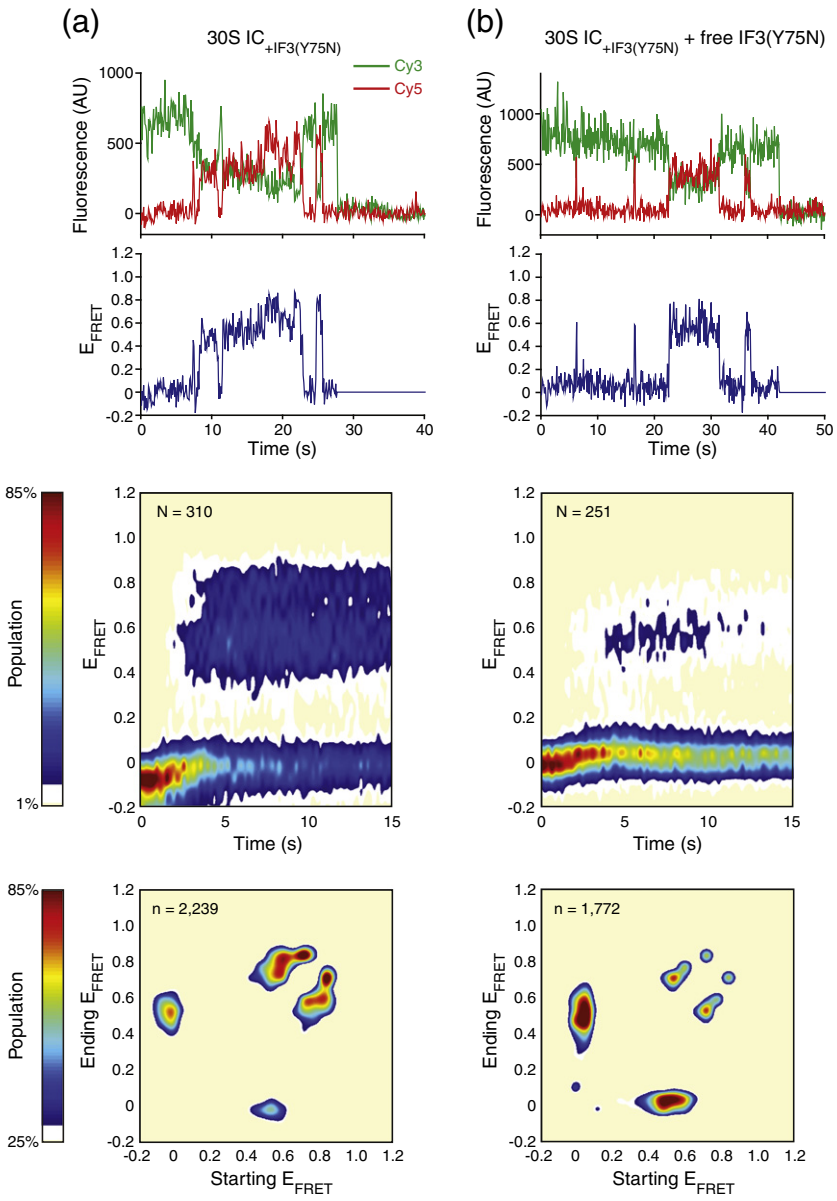

Fig. 6. Subunit joining to 30S $IC_{+IF3(Y75N)}$. Imaging buffer containing (Cy5)50S subunits (20 nM), IF1 (0.9 μM), and GTP (1 mM) was stopped-flow delivered to (Cy3)30S $IC_{+IF3(Y75N)}$ in the absence (a) or presence (b) of free IF3(Y75N) (0.9 μM). From top to bottom: Sample Cy3 and Cy5 fluorescence intensity *versus* time trajectories, the corresponding E_{FRET} *versus* time trajectories, time evolution of population FRET histograms, and TDPs. Data are plotted as described in the legend to Fig. 2.

signal due to rapid dissociation of (Cy3)IF2 and consequent signal loss at higher salt concentrations (Fig. S1), but it may be facilitated in the future by the utilization of a different, intersubunit smFRET signal [22,45].

The present results suggest that both inhibitory and productive conformations of 30S IC_{+IF3} are capable of recruiting the 50S subunit but that they differ in their ability to establish additional, stabilizing contacts. Initial recruitment of the 50S subunit to the 30S IC is most likely mediated through interactions between the GTP-bound form of IF2 and the peripheral L7/L12 stalk of the 50S subunit [16,18], after which IF2 can begin to establish contacts with the ribosomal RNA and protein components of the core of the 50S subunit and intersubunit bridges can begin to form at the interface between the 30S and 50S subunits. IF3 binds to the intersubunit surface of the platform domain of the 30S subunit, where numerous intersubunit bridges are located [19,20], which suggests that, in the inhibitory 30S IC_{+IF3} conformation, IF3 may sterically occlude a larger

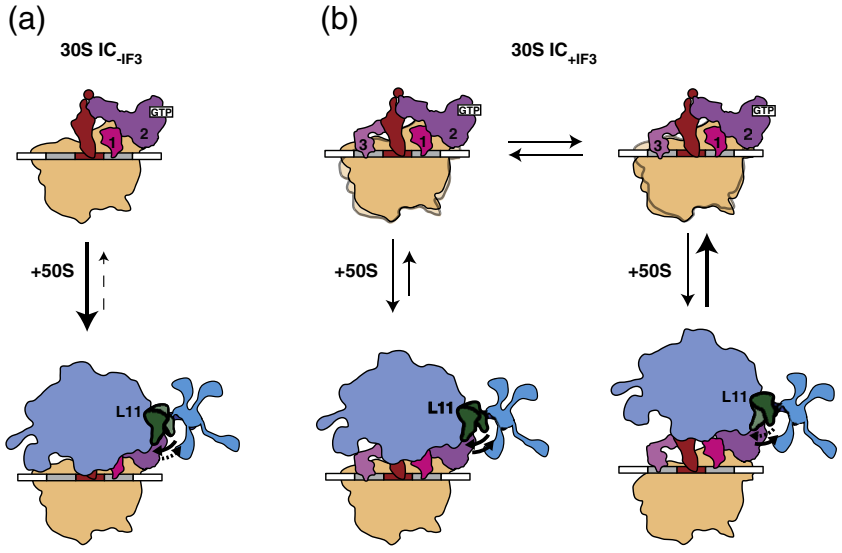

Fig. 7. Multiple modes of subunit joining in the absence and presence of IF3. Cartoon illustration of the three classes of subunit joining events identified in this study, which result in the formation of short-, intermediate-, and long-lifetime 70S ICs. At least two relative conformations between IF2 and L11 were sampled within the 70S ICs, characterized by E_{FRET} ratios of ~0.6 and ~0.8. Exchange between these conformational states is depicted in the cartoon as arising from movements of the L11 arm, though we note that the currently employed smFRET signal does not allow explicit determination of whether conformational rearrangements arise from movements of L11, IF2, or both. (a) Subunit joining to 30S IC_{-IF3} resulted in the formation of long-lifetime 70S ICs, which sampled E_{FRET} ratios of ~0.6 and ~0.8 and had an overall distribution weighted toward ~0.8. (b) Subunit joining to 30S IC_{+IF3} resulted in the formation of two classes of 70S ICs: An intermediate-lifetime 70S IC that samples E_{FRET} ratios of ~0.6 and ~0.8 to an approximately equal extent and a short-lifetime 70S IC that samples primarily E_{FRET} ratios centered around ~0.6. These two different classes of subunit joining are proposed to arise from two interconverting conformations of 30S IC_{+IF3}, each of which interacts differently with the incoming 50S subunit.

subset of the bridges than in the productive 30S IC_{+IF3} conformation.

In addition to the direct effects outlined in the previous paragraph, IF3 is also likely to influence the dynamics of subunit joining indirectly, by modulating the conformation and/or activities of other components of the 30S IC, including the 30S subunit, IF1, IF2, and fMet-$tRNA^{fMet}$. In this regard, the current smFRET data speak most directly to the effect of IF3 on the conformation and activity of IF2. They suggest that IF3 allosterically controls the positioning of IF2 on 30S IC_{+IF3}, causing IF2 to interact differently with the GAC upon subunit joining. At least two conformations of IF2 relative to the GAC were found to be accessible within the 70S IC, which comprise different distances between the fluorophore labeling positions on α-helix 8 of IF2 and the N-terminal domain of L11, characterized by E_{FRET} ratios centered at ~0.6 and ~0.8. Fluctuations between these two conformations were observed, which could arise from conformational changes of IF2 [30,31,46] and/or the L11 region [47–49] and could reflect changes in IF2–L11 interaction patterns or formation and disruption of IF2–L11 contacts. Notably, the increasing stability of the short-, intermediate-, and long-lifetime 70S ICs observed here is paralleled by an increase in occupancy of the ~0.8 FRET state (Fig. 4). This state could involve IF2–GAC contacts that contribute directly to overall 70S IC stability or that facilitate adjustment of the interface between the 30S and 50S subunits into an orientation conducive for intersubunit bridge formation.

Inclusion of high concentrations of free IF3 in our imaging buffer was found to result primarily in formation of short-lifetime 70S ICs (Fig. 5), which implies a shift in the putative 30S IC_{+IF3} conformational equilibrium toward high occupancy of the inhibitory conformation. A possible mechanistic explanation for how the presence of free IF3 could affect the conformational equilibrium of 30S IC_{+IF3}, which already contains a bound molecule of IF3, may be surmised by taking into account findings from recent single-molecule fluorescence studies on DNA binding proteins [40–42]. In these studies, protein molecules that were pre-bound to their DNA targets were observed to remain bound for long periods of time in the absence of free protein but to undergo accelerated turnover and rapid exchange with free protein molecules when the latter was included in solution [40,42]. The present results provide another example of a pre-bound protein whose biophysical behavior is affected by the absence or presence of free protein in solution. In analogy to the DNA binding proteins, it is possible

that a free molecule of IF3 could accelerate the turnover of a pre-bound molecule of IF3 by displacing it and concomitantly replacing it on 30S IC_{+IF3}. Such a mechanism might be expected to increase the occupancy of the inhibitory 30S IC_{+IF3} conformation if this conformation were associated with higher affinity IF3 binding compared to the productive 30S IC_{+IF3} conformation. Future single-molecule fluorescence experiments that directly monitor the effect of free IF3 on the dynamics and turnover of fluorophore-labeled IF3 that is pre-bound to 30S IC_{+IF3} will be required to test this and/or other possible mechanisms.

Modulation of the dynamic equilibrium between inhibitory and productive conformations of 30S IC_{+IF3} by free IF3 could provide a mechanism for the regulation of translation initiation efficiency. Shifts in the equilibrium toward the inhibitory conformation would result in formation of a larger fraction of short-lifetime 70S ICs, which may be either too transiently sampled or in a sub-optimal conformation for rapid binding of the first elongation factor (EF)-Tu-delivered aminoacyl-tRNA and entry of the 70S IC into translation elongation. The ability of free IF3 to bias the equilibrium toward the inhibitory conformation would then suggest that translation initiation efficiencies could be fine-tuned by spatial or temporal variations in the concentration of free IF3 in the cell. Indeed, *in vivo* experiments have shown that intracellular IF3 concentrations can affect initiation efficiency and fidelity: increased levels of spurious initiation on non-AUG start codons were observed when the concentration of IF3 was reduced, and decreased levels were observed when IF3 was overexpressed [50–52].

The notion that shifts in the 30S IC_{+IF3} conformational equilibrium could provide a mechanism for regulating translational fidelity at the level of initiation is further supported by smFRET data collected in the presence of the loss-of-function IF3(Y75N) mutant. 30S $IC_{+IF3(Y75N)}$ was found to participate in at least two modes of subunit joining, resulting in the formation of 70S ICs similar to the short- and intermediate-lifetime 70S ICs formed in the presence of wild-type IF3. However, IF3(Y75N) exhibited a reduced capacity to suppress formation of intermediate-lifetime 70S ICs, which could underlie the inability of IF3(Y75N) to repress translation from mRNAs containing atypical Class II start codons (e.g., CUG, AUU, AUC) and leaderless mRNAs *in vivo* [27,28].

In summary, by monitoring the subunit joining step of translation initiation using an smFRET approach, we have identified discrete modes of subunit joining that result in the formation of 70S ICs with different stabilities. IF3 plays a central role in influencing the strength of interactions formed between the 30S IC and the 50S subunit and likely does so by inducing and regulating a dynamic equilibrium between different conformations of 30S IC_{+IF3} that either inhibit or facilitate establishment of stabilizing intersubunit contacts. Although future investigations by cryo-EM and/or X-ray crystallography will be necessary to fully characterize the structural differences between these putative 30S IC_{+IF3} conformations, our smFRET data strongly suggest that they entail differential positioning of IF2 so as to influence its interactions with the GAC during 70S IC formation. IF3 binds to the 30S subunit at an early stage of 30S IC assembly [53,54], and most free 30S subunits are expected to contain bound IF3 *in vivo* [55]; thus, 30S IC_{+IF3} probably represents the predominant species of 30S IC participating in subunit joining in the cell. Control of 70S IC formation through modulation of the 30S IC_{+IF3} conformational equilibrium described here might therefore be leveraged to affect translational control at the level of initiation *in vivo*. Shifts in this equilibrium in response to factors such as IF3 concentration or different mRNA transcripts could modulate the rate of 70S IC formation and entry into translation elongation and could thus have important consequences for the regulation of translation initiation efficiency and fidelity.

Materials and Methods

Purification and fluorescent labeling of translation components

The IF2 construct used for smFRET experiments was generated by first introducing the S672C point mutation into a cloned copy of the γ-isoform of *E. coli* IF2 using the QuikChange II-E Site-Directed Mutagenesis Kit (Stratagene). Six-histidine-tagged IF2 S672C was purified by Ni-NTA chromatography, followed by cleavage of the affinity tag and purification by cation-exchange chromatography [56]. Fluorescent labeling was achieved by reaction with 10-fold molar excess of Cy3-maleimide followed by separation of (Cy3)IF2 from free dye with gel-filtration chromatography as previously described [56]. The labeling efficiency for (Cy3)IF2 was estimated to be ~90%. The γ-isoform of *E. coli* IF2 contains three wild-type cysteine residues, but control labeling reactions with wild-type IF2 demonstrated that these cysteines are not fluorescently labeled under the reactions conditions employed here.

Ribosomes were purified from the L11-deletion strain NVD005 or from the corresponding wild-type strain NVD001 [32,33], which were kindly provided by Prof. Walter Hill (University of Montana). 30S and 50S subunits were isolated by sucrose density gradient ultracentrifugation [56]. In order to generate (Cy5)50S subunits, six-histidine-tagged ribosomal protein L11 was first cloned, overexpressed, and purified using Ni-NTA chromatography followed by cleavage of the affinity tag. L11 was labeled at its wild-type cysteine residue (C39) by incubating ~15 nmol L11 with 0.2 mg Cy5-maleimide in 50 mM Na_2HPO_4 (pH 7.0), 100 mM NaCl, and 300 μM tris(2-carboxyethyl)phosphine hydrochloride for 2 h at room temperature followed by 4 °C overnight.

(Cy5)L11 was separated from free dye and unlabeled L11 using gel-filtration chromatography on a HiLoad Superdex 75 prep-grade column (GE Healthcare). Reconstitution of (Cy5)L11 with NVD005 50S subunits was performed following a procedure similar to that reported previously [57]. Briefly, 1 nmol of NVD005 50S subunits was mixed with 2 nmol of (Cy5)L11 in reconstitution buffer [50 mM Tris–Cl ($pH_{25\ °C}$ 7.6), 30 mM NH_4Cl, 70 mM KCl, 7 mM $MgCl_2$, and 1 mM DTT] and incubated at 37 °C for 15 min, followed by sucrose density purification. (Cy5)50S subunits were stored at −80 °C in 10 mM Tris–OAc ($pH_{25\ °C}$ 6.9), 60 mM NH_4Cl, 7.5 mM $Mg(OAc)_2$, 0.5 mM ethylenediaminetetraacetic acid (EDTA), and 6 mM β-mercaptoethanol.

All unlabeled initiation components, including IF1, IF3, and fMet-tRNA^{fMet}, were prepared as previously described [56]. Unless otherwise specified, the biotin-mRNA used in all microscope experiments (5′-Biotin-CAACCUAAAA CUUACACAAAUUAAAAAGGA*AAUAGAC***AUG**UUCAAA GUCGAAAAAUCUACUGCU-3′) and the non-biotin mRNA used in the initiation dipeptide formation assay (5′-GCAACCUAAAACUUACACAGGGCCCUAAG GA*AAUAAAA***AUG**UUUAAA-3′) were chemically synthesized and purchased from Dharmacon. In both mRNA sequences, the Shine–Dalgarno sequence is underlined, the spacer region is in italics, and the start codon is in boldface and is underlined.

Biochemical activity assays

The biochemical activities of (Cy3)IF2 and (Cy5)50S subunits were tested using a GTP hydrolysis assay and an initiation dipeptide formation assay to confirm that fluorescent labeling did not significantly interfere with their function (Figs. S2 and S3). These assays were performed in the same variant of Tris-polymix buffer used for smFRET experiments [10 mM Tris–OAc ($pH_{25\ °C}$ 7.5), 20 mM KCl, 1 mM NH_4OAc, 0.1 mM $Ca(OAc)_2$, 0.1 mM EDTA, 5 mM putrescine-HCl, 1 mM spermidine free base, 1% β-D-glucose, 15 mM $Mg(OAc)_2$, and 6 mM β-mercaptoethanol].

The GTP hydrolysis assay (Fig. S2) tests the ribosome-dependent GTPase activity of IF2 under multiple-turnover conditions, an activity that is known to be affected by the absence or presence of L11 within the 50S subunit [25]. The assay was performed by preparing 15 μL reactions in Tris-polymix buffer containing the following components (all concentrations are final after mixing): 30S subunits (0.4 μM); wild-type, L11(−), or (Cy5)-labeled 50S subunits (0.4 μM); wild-type or (Cy3) IF2 (0.8 μM); and a mixture of 25 μM GTP and 0.25 nM [α-^{32}P]GTP. The reaction was incubated at room temperature and 2-μL aliquots were removed and quenched with 2 μL of 100 mM EDTA (pH 9.5) at the indicated time points. [α-^{32}P]GDP was separated from [α-^{32}P]GTP using thin-layer chromatography, and the extent of GTP hydrolysis was quantified by phosphorimaging as previously described [56].

The initiation dipeptide formation assay was used to assess IF2-dependent formation of an elongation-competent 70S IC and subsequent formation of the first peptide bond (Fig. S3). Pre-formed 30S ICs were first prepared by mixing IF1 (0.9 μM), IF2 (0.9 μM, when included), GTP (1 mM), non-biotin mRNA (1.8 μM), 30S subunits (0.9 μM), and [^{35}S]fMet-tRNA^{fMet} (0.6 μM) in Tris-polymix buffer, incubating for 10 min at 37 °C, aliquoting, and flash-freezing. Next, two mixtures were prepared in Tris-polymix buffer, one containing the pre-formed 30S ICs and the other one containing either wild-type or Cy5-labeled 50S subunits and a pre-formed ternary complex composed of EF-Tu, GTP, and Phe-tRNA^{Phe} [EF-Tu(GTP)Phe-tRNA^{Phe}] that was prepared as previously described [56,58]. The two mixtures were incubated separately at room temperature for 5 min and then combined to start the reaction. The final reaction volume was 10 μL with final concentrations of 150 nM 30S ICs, 225 nM 50S subunits, and 600 nM EF-Tu(GTP)Phe-tRNA^{Phe} ternary complex. The reaction was incubated at room temperature and 2-μL aliquots were removed and quenched with 2 μL of 1 M KOH at the indicated time points. [^{35}S]fMet-Phe dipeptide product was separated from unreacted [^{35}S]fMet by electrophoretic thin-layer chromatography and the percent conversion to dipeptide was quantified by phosphorimaging as previously described [56].

Preparation and surface tethering of (Cy3)30S ICs

(Cy3)30S ICs were prepared by incubating IF1 (0.9 μM), (Cy3)IF2 (0.6 μM), GTP (1 mM), IF3 (0.9 μM, when included), fMet-tRNA^{fMet} (0.9 μM), 5′-biotin mRNA (1.8 μM), and NVD005 30S subunits (0.9 μM) in Tris-polymix buffer [21] [10 mM Tris-OAc ($pH_{25\ °C}$ 7.5), 20 mM KCl, 1 mM NH_4OAc, 0.1 mM $Ca(OAc)_2$, 0.1 mM EDTA, 5 mM putrescine-HCl, 1 mM spermidine free base, 1% β-D-glucose, 15 mM $Mg(OAc)_2$, and 6 mM β-mercaptoethanol] for 10 min at 37 °C. Aliquots of (Cy3)30S ICs were flash-frozen and stored at −80 °C prior to use.

Flow cells constructed from PEG and biotin-PEG-derivatized quartz microscope slides and glass coverslips were passivated with a mixture of 10 μM bovine serum albumin and 10 μM duplex DNA and treated with streptavidin as previously described [58]. (Cy3)30S ICs were then tethered to the surface of the flow cell through biotin-streptavidin interactions. (Cy3)30S IC_{-IF3} was diluted to ~100–200 pM and introduced into the flow cell in Tris-polymix buffer supplemented with IF1 (0.9 μM) and GTP (1 mM), followed by a 5-min incubation. The flow cell was then rinsed with the same buffer additionally supplemented with an oxygen scavenging system consisting of 50 U/mL glucose oxidase (Sigma) and 370 U/mL catalase (Sigma), as well as a triplet-state quencher cocktail consisting of 1 mM 1,3,5,7-cyclooctatetraene (Aldrich), 1 mM 3-nitrobenzyl alcohol (Fluka), and 1 mM Trolox (Sigma). (Cy3)30S IC_{+IF3} was diluted to ~1–4 nM and introduced into the flow cell in Tris-polymix buffer supplemented with IF1 (0.9 μM), IF3 (0.9 μM), GTP (1 mM), and fMet-tRNA^{fMet} (0.9 μM, when included) followed by a 5-min incubation. The flow cell was then rinsed with the same buffer additionally supplemented with oxygen scavenging system and triplet-state quencher cocktail.

smFRET experiments

smFRET experiments were performed using a wide-field, prism-based TIRF microscope [58–60]. A diode-pumped 532-nm laser (CrystaLaser) was used as an excitation source, operating at 6 mW as measured at the prism. Cy3 and Cy5 emissions were collected by a 1.2 NA 60× objective (Nikon), separated using a dual-view

imaging system (Photometrics), and detected using an electron-multiplying charge coupled device (Cascade II 512; Photometrics). Data were collected with 2-pixel binning at a frame rate of 10 s^{-1}. In a typical experiment, 40 μL of imaging buffer containing (Cy5)50S subunits and other initiation components in Tris-polymix buffer supplemented with oxygen scavenging system and triplet-state quencher cocktail was stopped-flow delivered into the flow cell at a rate of 0.39 mL/min using a custom-built syringe delivery system based off a programmable syringe pump (J-Kem Scientific), followed by the onset of data acquisition.

smFRET data analysis

Alignment of Cy3 and Cy5 channels, detection of colocalized Cy3 and Cy5 fluorescence signals, and generation of raw Cy3 and Cy5 fluorescence intensity *versus* time trajectories were performed using MetaMorph image analysis software (Molecular Devices). Cy3 and Cy5 fluorescence intensity *versus* time trajectories arising from single molecules were selected for analysis based on anti-correlation of Cy3 and Cy5 emission and single-step fluorophore photobleaching. The trajectories were corrected for bleed-through of Cy3 emission into the Cy5 channel and subsequently baseline corrected using custom scripts written in Matlab (MathWorks). E_{FRET} *versus* time trajectories were obtained by plotting $E_{FRET} = I_{Cy5}/(I_{Cy3} + I_{Cy5})$ at each time point, where I_{Cy3} and I_{Cy5} represent the bleed-through and baseline-corrected donor and acceptor emission intensities, respectively.

For dwell-time analysis, E_{FRET} *versus* time trajectories were idealized to a hidden Markov model using the vbFRET software package [61] and corrected for the estimated deadtime of our syringe delivery system (~500 ms). For each idealized trajectory, contiguous dwells with $E_{FRET} \leq 0.2$ were combined, and contiguous dwells with $E_{FRET} > 0.2$ were combined, in order to obtain dwell times in the zero-FRET state and aggregate non-zero FRET state, respectively. The last dwell of each idealized trace was not included in the analysis if it corresponded to the zero-FRET state due to potential effects from fluorophore photobleaching. The dwell times were used to construct plots of survival probabilities, in which the fraction of dwells for which $t_{dwell} \geq t$ was plotted *versus* t, where t_{dwell} is the dwell time and t is the time in seconds. These plots of survival probabilities were fit with single- or double-exponential decays in OriginPro 8 (Origin Lab Corp.) to obtain lifetimes and amplitudes of the zero-FRET state and aggregate non-zero FRET state. Single-exponential decays were of the form $y = \exp(-x/\tau)$ and double-exponential decays were of the form $y = A_1{*}\exp(-x/\tau_1) + (1 - A_1){*}\exp(-x/\tau_2)$. Errors on the lifetimes and amplitudes were obtained using a bootstrapping approach implemented in R in which the mean and standard deviation were calculated from 100 replicate data sets generated by sampling with replacement from the original distribution of dwell times. Reported values of $k_{a,app}$ were calculated by taking the inverse of the lifetime of the zero-FRET state and dividing by the concentration of (Cy5)50S subunits in the flow cell for the dataset collected at 20 nM (Cy5)50S subunits.

To quantify the percentage of short- and intermediate-lifetime 70S ICs observed for 30S IC_{+IF3}s containing wild-type IF3 *versus* IF3(Y75N), we defined short-lifetime 70S ICs to be dwells in the aggregate non-zero FRET state shorter than or equal to 2 s and defined intermediate-lifetime 70S ICs to be dwells in the aggregate non-zero FRET state longer than 2 s. This threshold was chosen because it provides optimal separation for two exponentially distributed populations with average lifetimes of 0.8 s and 10 s, which correspond to the estimated lifetimes of short- and intermediate-lifetime 70S ICs formed from 30S IC_{+IF3}s containing wild-type IF3.

Acknowledgments

This work was supported by grants from the Burroughs Wellcome Fund (CABS 1004856) and the US National Institutes of Health (R01 GM 084288) to R.L.G., as well as a Camille Dreyfus Teacher-Scholar Award to R.L.G. We thank Prof. Walter Hill for the kind gift of wild-type and L11-deletion strains used to purify ribosomes, as well as Prof. Bruno Klaholz for providing atomic coordinates of cryo-EM reconstructions of the 70S IC. We are grateful to members of the Gonzalez laboratory and the laboratory of Prof. Eric C. Greene for insightful discussions throughout the completion of this work. We would especially like to thank Dr. Kelvin Caban, Dr. Margaret Elvekrog, and Dr. Jiangning Wang for their valuable input.

Appendix A. Supplementary data

Supplementary data to this article can be found online at http://dx.doi.org/10.1016/j.jmb.2014.09.024.

Received 5 August 2014;
Received in revised form 22 September 2014;
Accepted 24 September 2014
Available online 13 October 2014

Keywords:
ribosome;
translation initiation;
70S initiation complex;
GTPase-associated center;
smFRET

Abbreviations used:
cryo-EM, cryogenic electron microscopy; EDTA, ethylenediaminetetraacetic acid; EF, elongation factor; FRET, fluorescence resonance energy transfer; GAC, GTPase-associated center; IC, initiation complex; IF, initiation factor; PEG, polyethylene glycol; smFRET, single-molecule fluorescence resonance energy tranfer; TDP, transition density plot; TIRF, total internal reflection fluorescence.

References

[1] Laursen BS, Sorensen HP, Mortensen KK, Sperling-Petersen HU. Initiation of protein synthesis in bacteria. Microbiol Mol Biol Rev 2005;69:101–23.

[2] Simonetti A, Marzi S, Jenner L, Myasnikov A, Romby P, Yusupova G, et al. A structural view of translation initiation in bacteria. Cell Mol Life Sci 2009;66:423–36.

[3] Antoun A, Pavlov MY, Lovmar M, Ehrenberg M. How initiation factors maximize the accuracy of tRNA selection in initiation of bacterial protein synthesis. Mol Cell 2006;23:183–93.

[4] Antoun A, Pavlov MY, Lovmar M, Ehrenberg M. How initiation factors tune the rate of initiation of protein synthesis in bacteria. EMBO J 2006;25:2539–50.

[5] Milon P, Konevega AL, Gualerzi CO, Rodnina MV. Kinetic checkpoint at a late step in translation initiation. Mol Cell 2008;30:712–20.

[6] Grigoriadou C, Marzi S, Pan D, Gualerzi CO, Cooperman BS. The translational fidelity function of IF3 during transition from the 30 S initiation complex to the 70 S initiation complex. J Mol Biol 2007;373:551–61.

[7] Hartz D, McPheeters DS, Gold L. Selection of the initiator tRNA by *Escherichia coli* initiation factors. Genes Dev 1989; 3:1899–912.

[8] Milon P, Carotti M, Konevega AL, Wintermeyer W, Rodnina MV, Gualerzi CO. The ribosome-bound initiation factor 2 recruits initiator tRNA to the 30S initiation complex. EMBO Rep 2010;11:312–6.

[9] Grigoriadou C, Marzi S, Kirillov S, Gualerzi CO, Cooperman BS. A quantitative kinetic scheme for 70 S translation initiation complex formation. J Mol Biol 2007;373:562–72.

[10] Hartz D, Binkley J, Hollingsworth T, Gold L. Domains of initiator tRNA and initiation codon crucial for initiator tRNA selection by *Escherichia coli* IF3. Genes Dev 1990;4:1790–800.

[11] Petrelli D, LaTeana A, Garofalo C, Spurio R, Pon CL, Gualerzi CO. Translation initiation factor IF3: two domains, five functions, one mechanism? EMBO J 2001;20:4560–9.

[12] Antoun A, Pavlov MY, Tenson T, Ehrenberg MM. Ribosome formation from subunits studied by stopped-flow and Rayleigh light scattering. Biol Proced Online 2004;6:35–54.

[13] Gualerzi CO, Pon CL. Initiation of mRNA translation in prokaryotes. Biochemistry 1990;29:5881–9.

[14] Boelens R, Gualerzi CO. Structure and function of bacterial initiation factors. Curr Protein Pept Sci 2002;3:107–19.

[15] Allen GS, Zavialov A, Gursky R, Ehrenberg M, Frank J. The cryo-EM structure of a translation initiation complex from *Escherichia coli*. Cell 2005;121:703–12.

[16] Huang C, Mandava CS, Sanyal S. The ribosomal stalk plays a key role in IF2-mediated association of the ribosomal subunits. J Mol Biol 2010;399:145–53.

[17] Naaktgeboren N, Schrier P, Moller W, Voorma HO. The involvement of protein L11 in the joining of the 30-S initiation complex to the 50-S subunit. Eur J Biochem 1976;62:117–23.

[18] Simonetti A, Marzi S, Billas IM, Tsai A, Fabbretti A, Myasnikov AG, et al. Involvement of protein IF2 N domain in ribosomal subunit joining revealed from architecture and function of the full-length initiation factor. Proc Natl Acad Sci U S A 2013;110:15656–61.

[19] Dallas A, Noller HF. Interaction of translation initiation factor 3 with the 30S ribosomal subunit. Mol Cell 2001;8:855–64.

[20] Julian P, Milon P, Agirrezabala X, Lasso G, Gil D, Rodnina MV, et al. The cryo-EM structure of a complete 30S translation initiation complex from *Escherichia coli*. PLoS Biol 2011;9:e1001095.

[21] Elvekrog MM, Gonzalez RL. Conformational selection of translation initiation factor 3 signals proper substrate selection. Nat Struct Mol Biol 2013;20:628–33.

[22] Marshall RA, Dorywalska M, Puglisi JD. Irreversible chemical steps control intersubunit dynamics during translation. Proc Natl Acad Sci U S A 2008;105:15364–9.

[23] Marshall RA, Aitken CE, Puglisi JD. GTP hydrolysis by IF2 guides progression of the ribosome into elongation. Mol Cell 2009;35:37–47.

[24] Tsai A, Petrov A, Marshall RA, Korlach J, Uemura S, Puglisi JD. Heterogeneous pathways and timing of factor departure during translation initiation. Nature 2012;487:390–3.

[25] Brandi L, Marzi S, Fabbretti A, Fleischer C, Hill WE, Gualerzi CO, et al. The translation initiation functions of IF2: targets for thiostrepton inhibition. J Mol Biol 2004;335:881–94.

[26] Qin H, Grigoriadou C, Cooperman BS. Interaction of IF2 with the ribosomal GTPase-associated center during 70S initiation complex formation. Biochemistry 2009;48:4699–706.

[27] Sussman JK, Simons EL, Simons RW. *Escherichia coli* translation initiation factor 3 discriminates the initiation codon *in vivo*. Mol Microbiol 1996;21:347–60.

[28] Maar D, Liveris D, Sussman JK, Ringquist S, Moll I, Heredia N, et al. A single mutation in the IF3 N-terminal domain perturbs the fidelity of translation initiation at three levels. J Mol Biol 2008;383:937–44.

[29] Nyengaard NR, Mortensen KK, Lassen SF, Hershey JW, Sperling-Petersen HU. Tandem translation of *E. coli* initiation factor IF2 beta: purification and characterization *in vitro* of two active forms. Biochem Biophys Res Commun 1991;181:1572–9.

[30] Roll-Mecak A, Cao C, Dever TE, Burley SK. X-Ray structures of the universal translation initiation factor IF2/eIF5B: conformational changes on GDP and GTP binding. Cell 2000;103:781–92.

[31] Myasnikov AG, Marzi S, Simonetti A, Giuliodori AM, Gualerzi CO, Yusupova G, et al. Conformational transition of initiation factor 2 from the GTP- to GDP-bound state visualized on the ribosome. Nat Struct Mol Biol 2005;12:1145–9.

[32] Van Dyke N, Xu W, Murgola EJ. Limitation of ribosomal protein L11 availability *in vivo* affects translation termination. J Mol Biol 2002;319:329–39.

[33] Bowen WS, Van Dyke N, Murgola EJ, Lodmell JS, Hill WE. Interaction of thiostrepton and elongation factor-G with the ribosomal protein L11-binding domain. J Biol Chem 2005; 280:2934–43.

[34] The PyMOL Molecular Graphics System, Version 1.3, Schrödinger, LLC.

[35] Tomsic J, Vitali LA, Daviter T, Savelsbergh A, Spurio R, Striebeck P, et al. Late events of translation initiation in bacteria: a kinetic analysis. EMBO J 2000;19:2127–36.

[36] Antoun A, Pavlov MY, Andersson K, Tenson T, Ehrenberg M. The roles of initiation factor 2 and guanosine triphosphate in initiation of protein synthesis. EMBO J 2003;22:5593–601.

[37] Grunberg-Manago M, Dessen P, Pantaloni D, Godefroy-Colburn T, Wolfe AD, Dondon J. Light-scattering studies showing the effect of initiation factors on the reversible dissociation of *Escherichia coli* ribosomes. J Mol Biol 1975;94:461–78.

[38] Chaires JB, Pande C, Wishnia A. The effect of initiation factor IF-3 on *Escherichia coli* ribosomal subunit association kinetics. J Biol Chem 1981;256:6600–7.

[39] Ha T. Single-molecule approaches embrace molecular cohorts. Cell 2013;154:723–6.

[40] Graham JS, Johnson RC, Marko JF. Concentration-dependent exchange accelerates turnover of proteins bound to double-stranded DNA. Nucleic Acids Res 2011;39:2249–59.

[41] Joshi CP, Panda D, Martell DJ, Andoy NM, Chen TY, Gaballa A, et al. Direct substitution and assisted dissociation pathways for turning off transcription by a MerR-family metallor-egulator. Proc Natl Acad Sci U S A 2012;109:15121–6.
[42] Gibb B, Ye LF, Gergoudis SC, Kwon Y, Niu H, Sung P, et al. Concentration-dependent exchange of replication protein A on single-stranded DNA revealed by single-molecule imaging. PLoS One 2014;9:e87922.
[43] O'Connor M, Gregory ST, Rajbhandary UL, Dahlberg AE. Altered discrimination of start codons and initiator tRNAs by mutant initiation factor 3. RNA 2001;7:969–78.
[44] Simonetti A, Marzi S, Myasnikov AG, Fabbretti A, Yusupov M, Gualerzi CO, et al. Structure of the 30S translation initiation complex. Nature 2008;455:416–20.
[45] Ermolenko DN, Majumdar ZK, Hickerson RP, Spiegel PC, Clegg RM, Noller HF. Observation of intersubunit movement of the ribosome in solution using FRET. J Mol Biol 2007;370:530–40.
[46] Eiler D, Lin J, Simonetti A, Klaholz BP, Steitz TA. Initiation factor 2 crystal structure reveals a different domain organization from eukaryotic initiation factor 5B and mechanism among translational GTPases. Proc Natl Acad Sci U S A 2013;110:15662–7.
[47] Rawat U, Gao H, Zavialov A, Gursky R, Ehrenberg M, Frank J. Interactions of the release factor RF1 with the ribosome as revealed by cryo-EM. J Mol Biol 2006;357:1144–53.
[48] Schuwirth BS, Borovinskaya MA, Hau CW, Zhang W, Vila-Sanjurjo A, Holton JM, et al. Structures of the bacterial ribosome at 3.5 Å resolution. Science 2005;310:827–34.
[49] Kavran JM, Steitz TA. Structure of the base of the L7/L12 stalk of the *Haloarcula marismortui* large ribosomal subunit: analysis of L11 movements. J Mol Biol 2007;371:1047–59.
[50] Butler JS, Springer M, Dondon J, Graffe M, Grunberg-Manago M. *Escherichia coli* protein synthesis initiation factor IF3 controls its own gene expression at the translational level *in vivo*. J Mol Biol 1986;192:767–80.
[51] Olsson CL, Graffe M, Springer M, Hershey JW. Physiological effects of translation initiation factor IF3 and ribosomal protein L20 limitation in *Escherichia coli*. Mol Gen Genet 1996;250:705–14.
[52] Sacerdot C, Chiaruttini C, Engst K, Graffe M, Milet M, Mathy N, et al. The role of the AUU initiation codon in the negative feedback regulation of the gene for translation initiation factor IF3 in *Escherichia coli*. Mol Microbiol 1996;21:331–46.
[53] Karimi R, Pavlov MY, Buckingham RH, Ehrenberg M. Novel roles for classical factors at the interface between translation termination and initiation. Mol Cell 1999;3:601–9.
[54] Milon P, Maracci C, Filonava L, Gualerzi CO, Rodnina MV. Real-time assembly landscape of bacterial 30S translation initiation complex. Nat Struct Mol Biol 2012;19:609–15.
[55] Zucker FH, Hershey JW. Binding of *Escherichia coli* protein synthesis initiation factor IF1 to 30S ribosomal subunits measured by fluorescence polarization. Biochemistry 1986; 25:3682–90.
[56] Fei J, Wang J, Sternberg SH, MacDougall DD, Elvekrog MM, Pulukkunat DK, et al. A highly purified, fluorescently labeled *in vitro* translation system for single-molecule studies of protein synthesis. Methods Enzymol 2010;472:221–59.
[57] Seo HS, Abedin S, Kamp D, Wilson DN, Nierhaus KH, Cooperman BS. EF-G-dependent GTPase on the ribosome. conformational change and fusidic acid inhibition. Biochemistry 2006;45:2504–14.
[58] Blanchard SC, Kim HD, Gonzalez RL, Puglisi JD, Chu S. tRNA dynamics on the ribosome during translation. Proc Natl Acad Sci U S A 2004;101:12893–8.
[59] Fei J, Kosuri P, MacDougall DD, Gonzalez RL. Coupling of ribosomal L1 stalk and tRNA dynamics during translation elongation. Mol Cell 2008;30:348–59.
[60] Blanchard SC, Gonzalez RL, Kim HD, Chu S, Puglisi JD. tRNA selection and kinetic proofreading in translation. Nat Struct Mol Biol 2004;11:1008–14.
[61] Bronson JE, Fei J, Hofman JM, Gonzalez RL, Wiggins CH. Learning rates and states from biophysical time series: a Bayesian approach to model selection and single-molecule FRET data. Biophys J 2009;97:3196–205.